ACS APPLIED MATERIALS & INTERFACES

Research Article

www.acsami.org

Vertical p-Type Cu-Doped ZnO/n-Type ZnO Homojunction Nanowire-Based Ultraviolet Photodetector by the Furnace System with Hotwire Assistance

Cheng-Liang Hsu,*[,†] Yi-Dian Gao,[†] You-Syuan Chen,[†] and Ting-Jen Hsueh*[,‡]

[†]Department of Electrical Engineering, National University of Tainan, Tainan 700, Taiwan, Republic of China

[‡]National Nano Device Laboratories, Tainan 741, Taiwan, Republic of China

ABSTRACT: Vertical p-ZnO:Cu/n-ZnO homojunction nanowires (NWs) and whole ZnO:Cu NWs were synthesized on a ZnO thin film/glass substrate by a furnace at 600 °C with 1700 °C hotwire assistance. According to the ZnO:Cu NW investigation, the energy-dispersive X-ray (EDX) spectrum indicates that the Cu content is 3.01 atomic %. The X-ray diffraction (XRD) peaks of ZnO:Cu NWs shift toward larger angles with increasing amounts of doped Cu. The Cu dopant enhanced the photoluminescence (PL) green-band peak and decreased the conductivity of the NWs, as measured by *I*−*V*. The gas sensing measurement and Hall effect verified that all ZnO:Cu NWs were p-type. In this study, transmission electron microscopy (TEM) and EDX mapping images revealed that the majority of the Cu element is located at the top of the p-ZnO:Cu/n-ZnO NW. The high-resolution transmission electron microscopy (HRTEM) image of the p-ZnO:Cu region shows that the NWs are [0001] growth-oriented, with lateral surfaces enclosed by ($\bar{1}$101) planes. The *I*−*V* curve of p-ZnO:Cu/n-ZnO NWs displays the characteristics of normal rectifying diodes. The photocurrent under ultraviolet (UV) exposure was around 6 times higher than the dark current at the reverse bias of −5 V.

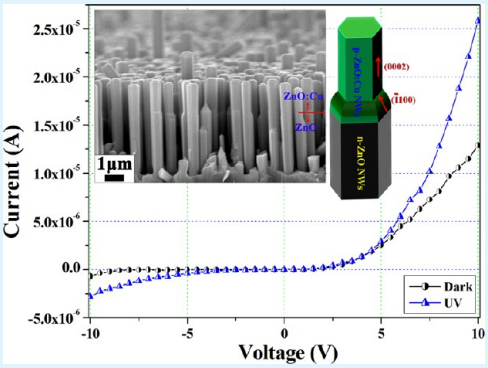

KEYWORDS: *Cu-doped ZnO, p-type, nanowires, homojunction, hotwire*

INTRODUCTION

Recently, zinc oxide (ZnO) has attracted much interest, owing to its potential applications in optoelectronic, electronic, and piezoelectric devices.[1−5] ZnO is a kind of II−VI compound material featuring a wide band gap of 3.3 eV and a large exciton binding energy of about 60 meV at 25 °C. Doping is an important and effective way of improving semiconductor properties. Up to now, It is well-known that the most suitable dopant for p-type doping in ZnO is the Group 5 elements [nitrogen (N), phosphorus (P), arsenic (As), and antimony (Sb)] substituting for oxygen.[5−11] In comparison to Group 5, there have been few p-type reports discussing Group 11 [copper (Cu), silver (Ag), and Gold (Au)] doping at the Zn sites that offer +1 valence.[12−16] The Group 11 elements can assume a valence of either +1 or +2, depending upon their chemical configuration. The low formation energy and high ionization energy of Cu have limited thermodynamic equilibrium solubility in ZnO. The Cu-doped ZnO (ZnO:Cu) can be synthesized by various technologies, such as vapor-phase transport,[16] pulsed-laser deposition,[17] radio frequency (RF) magnetron sputtering,[18] plasma-assisted molecular beam epitaxy (PA-MBE),[13] and electrochemical deposition.[19] The radii of Cu^+ (77 pm) and Cu^{2+} (73 pm) ions are smaller than Ag^+ ions (115 pm) and are, thus, suitable for Zn^{2+} (74 pm) ion substitution, which has a similar size. The Cu dopants substituted at the Zn sites have been reported to exhibit acceptor states in the ZnO band gap located at −0.17 eV below the conduction band (E_C) bottom and +0.45 eV above the valence band (E_V).[19−21]

ZnO is an intrinsically n-type semiconductor, owing to the presence of zinc interstitials or oxygen vacancies; however, fabrication of stable and reproducible p-type ZnO is troublesome, which makes the p−n homojunction fabrication challenging in a ZnO nanowire (NW) base. In past years, there have been many reports related to the heterojunction employing n-type ZnO NWs on p-type substrates, such as Si, GaN, SiC, and NiO.[22−25] Among these, GaN is the most commonly used for heterojunction applications, which is because ZnO and GaN have similar lattice constants with the same wurtzite structure. Regardless of how simply the p−n heterojunction was manufactured, the p−n homojunction has a stronger physical structure and more stable chemical bonding. Some research teams have completed homojunctions using n-ZnO thin-film epitaxial growth on p-type ZnO thin-film structures.[26] A few other researchers have completed homojunctions in NWs using p-type P and N dopant resources.[27−29] This paper suggests a means of overcoming the NW homojunction challenge and temperature limitations of

Received: December 29, 2013
Accepted: February 28, 2014
Published: February 28, 2014

   dx.doi.org/10.1021/am406030d | ACS Appl. Mater. Interfaces 2014, 6, 4277−4285

furnace tubes, resulting in successful synthesis of well-aligned p-type Cu-doped ZnO (p-ZnO:Cu)/n-type ZnO homojunction NWs on ZnO/glass substrates employing inexpensive equipment. In this investigation, a p−n homojunction diode was assembled using p-ZnO:Cu/n-ZnO NWs. Physical properties of the p-ZnO:Cu/n-ZnO homojunction NWs and the electro-optic properties of the fabricated photodetector will also be discussed.

EXPERIMENTAL SECTION

Figure 1 schematically depicts the furnace system with hotwire assistance. A ZnO film buffer layer of approximately 50 nm was deposited by RF magnetron sputtering on glass substrates (Corning 1737). The target was ZnO (99.996%), and the base pressure was 7.6×10^{-6} Torr. The total pressure (argon) was maintained at 1.3×10^{-3} Torr during sputtering, while the substrate temperature was kept at 80 °C. The ZnO buffer layer deposition rate was around 3.2 nm/min. The NWs were performed by vapor phase transport deposition onto the ZnO buffer layer by a furnace system with hotwire assistance. The zinc vapor source is Zn metal powder with a purity of 99.9% from Strem Chemicals. The substrates and zinc vapor source in an alumina boat were inserted into the quartz tube and put closely in the middle of the furnace. The diameter and length of the quartz tube were 5 and 120 cm, which is the standard specification size of the vendor. In this study, the diameter and length of the Ta wire (99.996% purity) were 0.8 and 20.0 mm, respectively. Cu foil (99.93% purity) was placed close to Ta hotwires and provided the required dopant source. The melting point of 3017 °C for the Ta wire is higher than that of the Cu foil at 1084.6 °C, which ensures that Ta vapor diffusion mixing with Cu vapor at the hotwire working temperature does not occur. Gaseous argon flow [54 standard cubic centimeters per minute (sccm)] is the carry gas into the furnace with a small amount oxygen (0.8 sccm). Oxygen is reactive with Zn vapor to synthesize ZnO NWs. During the growth of the ZnO:Cu NWs, the furnace temperature, the pressure in the quartz tube, and synthesis time were maintained at 600 °C, 8.7 Torr, and 30 min, respectively. As the furnace tube started heating, the hotwire system temperature was increased to around 1400 °C (sample A) or 1700 °C (sample B). The ZnO:Cu/n-ZnO homojunction NWs were prepared in the same furnace conditions. When the temperature of the furnace was raised to 600 °C after 10 min, the hotwire power supply was turned on and the Ta hotwire temperature increased to 1700 °C. According to the optimized process conditions, we have successfully manufactured more than a dozen samples. The manufacturing yield is about 20%. Because this synthesis equipment is handmade, this is relatively poor process stability. Using a high-precision equipment will have the opportunity to substantially increase yields.

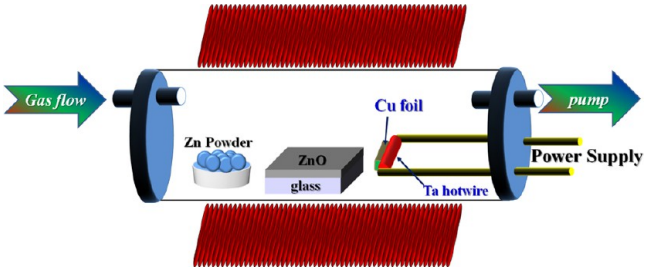

Figure 1. Schematic depiction of the furnace system with hotwire assistance.

Figure 2 schematic diagrams the processing steps that were implemented in this investigation; photodetector were manufactured by these steps. After these ZnO:Cu NWs had grown, the polymerization of methyl methacrylate (PMMA) material acted as a barrier layer and covered the surface of the NW sample by spin coating (800 rpm/15 s). The electrode regions were defined with photolithography and etch processes, after which silver paste was coated on these electrode regions. These samples were then annealed at 110 °C for 15 min in an Ar ambient atmosphere to form a good ohmic contact. The surface morphologies and crystallinity of ZnO:Cu NWs were measured and analyzed by field emission scanning electron microscopy (FESEM, JEOL-JSM7000F) and X-ray diffraction (XRD, MAC-MXP18). The crystalline structure and element distribution were observed with high-resolution transmission electron microscopy (HRTEM, JEOL-JEM2100F). Magnetization measurements were carried out using a superconducting quantum interference device (SQUID) vibrating sample magnetometer (VSM).

RESULTS AND DISCUSSION

The cross-sectional SEM images of samples A and B were shown in panels a and b of Figure 3, respectively. The magnified images of panels a and b of Figure 3 were inserted in their top-left-hand corner. The vertical, uniform, high-density ZnO:Cu NWs were grown on a ZnO/glass substrate at 600 °C.

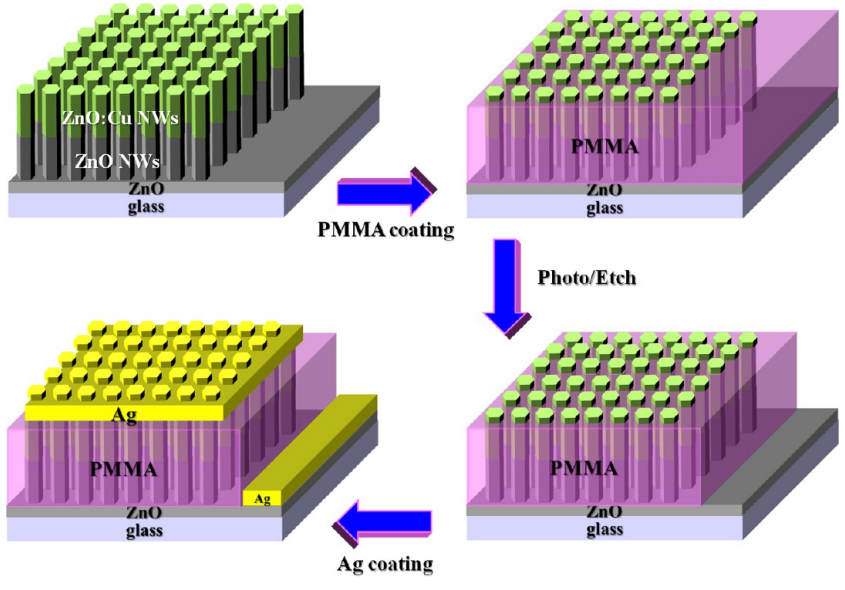

Figure 2. Schematic diagrams of the processing steps that were implemented in this study.

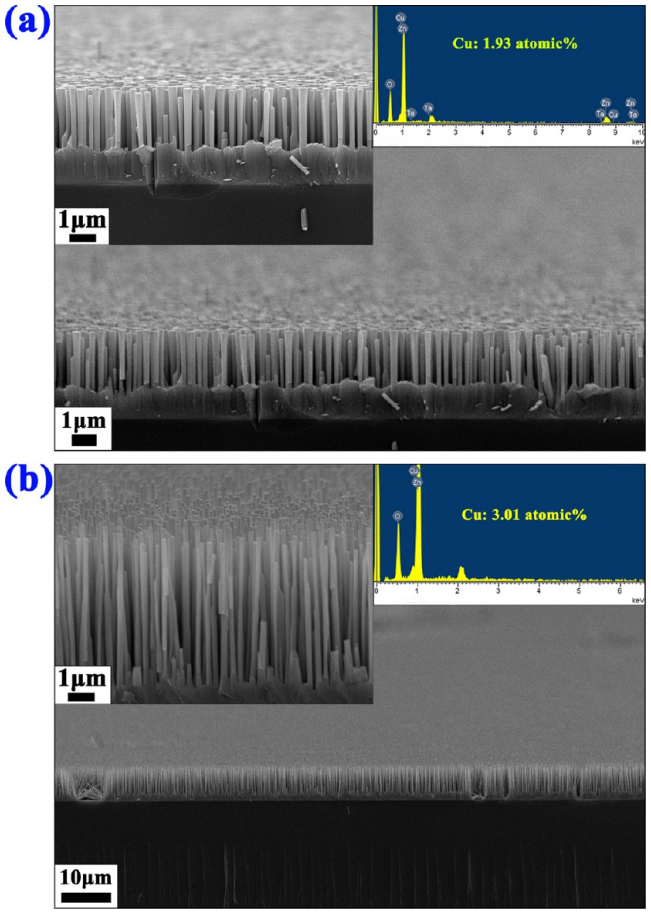

Figure 3. Cross-sectional FESEM images of (a) sample A (hotwire ~ 1400 °C) and (b) sample B (hotwire ~ 1700 °C). Insets in left- and right-hand corners are the magnified image and EDX spectrum, respectively.

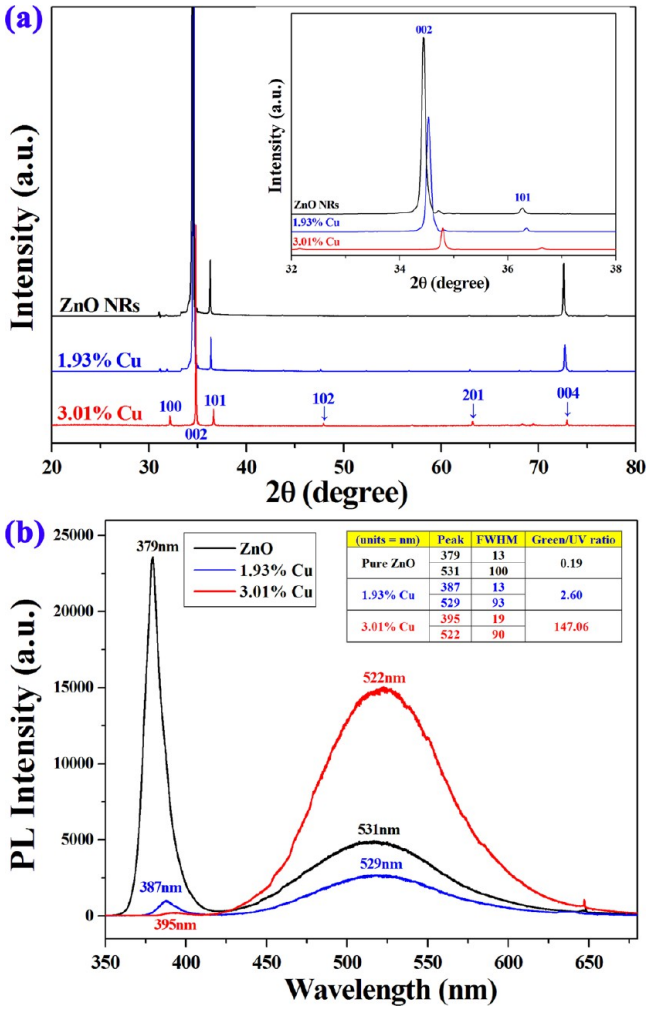

Figure 4. (a) XRD 2θ scan spectra and (b) PL spectra of the ZnO NW and Cu-doped ZnO NW samples at room temperature.

The lengths of the ZnO:Cu NWs of samples A and B are around 2.3 and 5.5 μm, respectively, the diameters of which are 150−400 and 100−180 nm, respectively. The insets in their top-right-hand corner of panels a and b of Figure 3 reveal the energy-dispersive X-ray (EDX) spectroscopy of samples A and B from the randomly picked. It is clearly observed that signals originated from Zn, Cu, and O elements. The intensity of Zn, O, and Cu peak ratio can be calculated by the Cu content of samples A and B. The Cu contents of samples A and B are 1.93 and 3.01 atomic %, respectively. Because the Ta hotwire temperatures of samples A and B are 1400 and 1700 °C, sample B should contain a higher Cu concentration because of its larger Cu vapor with a higher hotwire temperature. The higher Cu doping causes a longer and narrower NW.

Figure 4a depicts the XRD spectrum of pure ZnO and 1.93 and 3.01% Cu-containing NW samples. The crystallographic characteristics of these NWs demonstrated the hexagonal wurtzite structures. The highest intensity of the XRD peak is (002) and verifies the NW growth preferential orientation on the *c* axis. The formation of Cu_2O, CuO, or Cu phases was not detected within the sensitivity of the XRD, which implies that Cu atoms may replace Zn atomic sites substitutionally or incorporate interstitially in the hexagonal lattices. The inset of Figure 4a displays that ZnO:Cu peaks were shifted to a larger angle by the examined (002) and (101) peak positions. Pure ZnO and 1.93 and 3.01% Cu-containing NW samples yielded strong (002) peaks at about 34.44°, 34.53°, and 34.80°, respectively. Moreover, the ZnO peak shifts to larger angles with an increasing amount of doped Cu because of the ionic radius of Cu^{2+} (0.73 Å) being smaller than that of Zn^{2+} (0.74 Å). The verified doped copper element mostly came from Cu^{2+} and less Cu^{+} (77 pm). The (002) peaks of 1.93 and 3.01% Cu-containing NWs were shifted by approximately 0.09° and 0.36°, respectively, which are equal to the reduction of the lattice constant by 0.25 and 1.01%. This result is similar to observations that have been made for ZnO:Cu thin films and nanostructures.[16−21]

Figure 4b depicts the photoluminescence (PL) spectra of pure ZnO and 1.93 and 3.01% Cu-containing samples at room temperature. It exhibits strong peaks at approximately 379, 387, and 395 nm, with full width at half maximum (FWHM) of 13, 13, and 19 nm, respectively. The ultraviolet (UV) emission peaks of these NW samples underwent transitions near the 3.3 eV ZnO band gap; therefore, these corresponding UV emissions are generally ascribed to the recombination of excitons via an exciton−exciton collision process.[30] With an increasing Cu concentration, the UV emission peak intensity decreases and the peak red shift increases. This indicates that increasing the Cu concentration causes the narrowing band gap of ZnO NWs, which is a well-known general phenomenon in semiconductors. The Cu dopants substituted at the Zn sites

dx.doi.org/10.1021/am406030d | ACS Appl. Mater. Interfaces 2014, 6, 4277−4285

have been reported to exhibit acceptor states in the ZnO band gap situated at −0.17 eV under the E_C bottom and +0.45 eV above the E_V.[16−21] With an increase in the amount of Cu doping, the density of these dopant states increase and form a continuous state. This is in the band gap, and effectively, the band gap decreases. The PL peaks of pure ZnO and 1.93 and 3.01% Cu-containing samples were found to be strong peaks at 531, 529, and 522 nm, with FWHM of 100, 93, and 90 nm, respectively. The width of these green band peaks is broader than UV emission. Deep level emission (green band) peaks of around 2.35 eV (522−531 nm) come from Cu dopants and the oxygen defect formation.[31] The UV emission peak/green emission peak ratio of ∼147.06 for the 3.01% Cu-containing sample is larger than that for either the 1.93% Cu-containing (∼2.69) or ZnO (∼0.19) samples. The Cu dopant enhanced the green band peak and increased the ionized oxygen vacancy in ZnO.

The natural p-type semiconductor CuO and Cu_2O band gaps are 1.2 and 2.1 eV, respectively. It is possible to decrease the band gap of the ZnO gap by alloying it with a smaller band gap CuO and Cu_2O, but the formation of Cu_2O, CuO, or Cu phases was not detected within the sensitivity of the XRD. All XRD peaks are the ZnO structure. The lattice parameters and structures of CuO and Cu_2O have a big difference from ZnO, which is difficult to keep ZnO NW vertical growth. The Cu atoms may replace Zn atomic sites substitutionally or incorporate interstitially in the hexagonal lattices. The major dopant came from Cu^{2+} by the XRD shift to a larger angle result.

Figure 5a plots the current−voltage (I−V) characteristics of these NWs in the ambient atmosphere at room temperature. The Ag electrode and Ag/NW contact resistances can be neglected because these resistances are lower than NWs. Thereby, the resistance variation came only from the NW resistance variation. The highest measured currents of pure ZnO and 1.93 and 3.01% Cu-containing samples were 1.86×10^{-5}, 6.20×10^{-7}, and 3.05×10^{-7} A at the bias of 10 V, respectively. The ZnO sample was around 60.1 times that of the 3.01% Cu-containing sample. The possible interpretation is that Cu impurities decreased the conductivity of the NWs. The measured current was increasing linearly with the increasing voltage. The resistances between the NWs and electrodes confirmed the ohmic contact.

Figure 5b plots the repeated responses of the 3.01% Cu-containing sample to 100 ppm ethanol at 110 °C. The environmental humidity was 55%. As seen, the measured current was decreased with the ethanol concentration increased at 110 °C. The property of the sensing response is performance of a strongly p-type characteristic. Below 150 °C, the O_2^- molecular species dominates, as demonstrated by temperature-programmed desorption (TPD), Fourier transform infrared spectroscopy (FTIR) and electron spin resonance (ESR).[32] The hole concentration of the p-ZnO:Cu NW surface was increased rapidly because of the oxygen-captured free electrons.

$$O_{2(ads)} + e^- \leftrightarrows O_2^-$$

The next reaction step includes the oxygen ionic species and ethanol. The reaction is proceeding through a path as follows:[5]

$$C_2H_5OH_{(gas)} + 3O_2^- \leftrightarrows 3CO_{2(gas)} + 3H_2O_{(gas)} + 3e^-$$

The oxygen ionic species and ethanol are reactive to produce a plethora of electrons. These electrons were recombinations with holes and then decreased the hole concentration at the NW surfaces. Accordingly, the conductivity of NWs is rapidly decreasing. The sensing response and recovery timing are stable and quick, which demonstrates that the sensing performance of NWs was favorable.

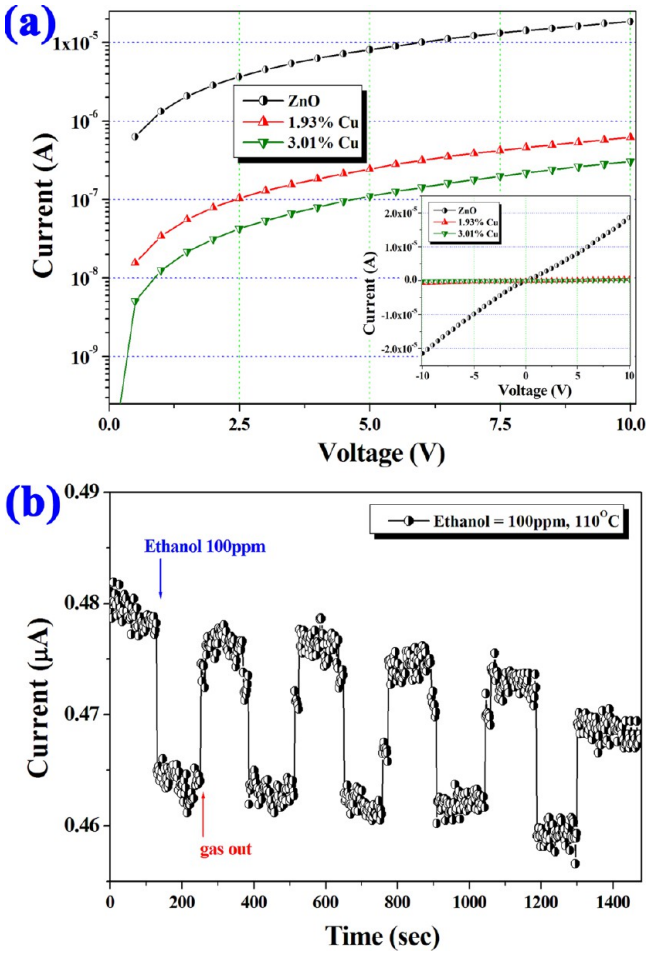

Figure 5. (a) I−V property of the ZnO NW and Cu-doped ZnO NW samples. (b) Responses of the ZnO:Cu NW sensor to extracting and implanting ethanol gas at 110 °C.

The 3.01% Cu-containing sample exhibited a p-type characteristic by the Hall effect measurement. The electrical properties of the ZnO:Cu sample were as follows: Hall mobility, 11.5 $cm^2\ V^{-1}\ s^{-1}$; sheet resistance, 26.35 Ω/square; and hole concentration (p), $8.96 \times 10^{15}\ cm^{-3}$. The ZnO:Cu sample has high Cu, containing 3.01 atomic %, but its hole concentration is very low, $\sim 10^{16}\ cm^{-3}$. ZnO is natively n-type, which is very hard to transfer to p-type with dope technology. The Hall effect and gas sensing measurement verified that the ZnO:Cu NWs were p-type. The dopant Cu^+ ions decrease the electron concentration of ZnO NWs, which increase the resistance of ZnO:Cu NWs.

Figure 6 displays magnetization−magnetic field (M−H) curves measured for the 1.93 and 3.01% Cu-containing samples. The left-hand corner inset is the magnified image. These samples exhibit clear hysteresis loops and suggest the room-temperature ferromagnetism (RTFM) property. The magnetization of the 3.01% Cu-containing sample is higher than that of the 1.93% Cu-containing sample. The right-hand corner inset shows the temperature-dependent (2−300 K) magnetization of the samples at 1500 Oe. The temperature-dependent magnetization image was inserted in the bottom-right-hand corner of

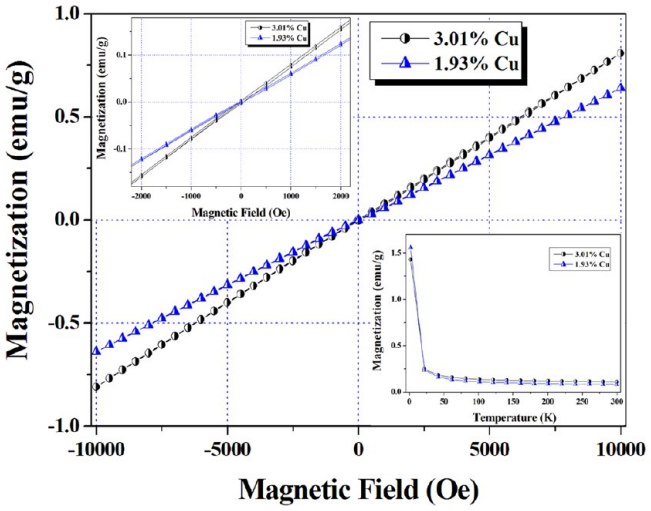

Figure 6. Magnetic properties of the 1.93 and 3.01% Cu-containing samples. The insets in left- and right-hand corners are the magnified image and temperature-dependent magnetization of the samples at 1500 Oe, respectively.

Figure 6a. The 3.01% Cu-containing sample is stronger than that of the 1.93% Cu-containing sample. These ZnO:Cu samples display the Curie–Weiss magnetic behavior at lower temperatures. The presence of the paramagnetic phase is most likely owing to the localized character of Cu 3d electrons and the dynamic Jahn–Teller (DJT) effect.[33] Additionally, Spaldin et al. forecasted that transition-metal-element-doped ZnO will be a strong ferromagnetic material.[34] Past papers have suggested that similar magnetization exists in p-type ZnO:Cu NWs or thick films.[16]

Figure 7a depicts the fabrication process of the p-ZnO:Cu/n-ZnO homojunction NWs. The vapor phase transports deposition growth without metal catalysis. The Zn melting point is 419.5 °C; as such, the major source of the formation ZnO NWs is Zn vapor with oxygen at 419.5–600 °C. The n-ZnO NWs typically grew along the columnar grains of the ZnO buffer layer at temperatures above 500 °C. As the temperature was raised to 600 °C after 10 min, the high-power supply to heat the Ta hotwire was turned on and increased to 1700 °C. The amount of Cu vapor rapidly increased as the temperature increased. The Cu vapor was diffused, blended with Zn vapor, and then reacted with oxygen to grow the p-ZnO:Cu NWs. Cu-doped ZnO NWs along with the original vertical p-ZnO NWs continued to grow. The final composition of the NWs was made from two parts, namely, p-ZnO:Cu and n-ZnO. Figure 7b reveals the cross-sectional SEM images of the p-ZnO:Cu/n-ZnO homojunction NWs. The inset in the top-left-hand corner of Figure 7b reveals an enlarged image. The diameter and length of the p-ZnO:Cu/n-ZnO NWs are approximately 5.2 μm and 200–500 nm, respectively, while the length of the p-ZnO:Cu region is around 1.75 μm. The diameter of the p-ZnO:Cu region is narrower than that of the n-ZnO region by about 30–50 nm. The vertical, uniform, high-density p-ZnO:Cu/n-ZnO homojunction NWs were synthesized on a ZnO/glass substrate.

Figure 8a displays that cross-sectional TEM and EDX mapping images of p-ZnO:Cu/n-ZnO homojunction NWs. TEM sample preparation methods have been published in previous work.[5] High concentrations of Zn and O elements are evenly distributed on the NW. The p-ZnO:Cu/n-ZnO

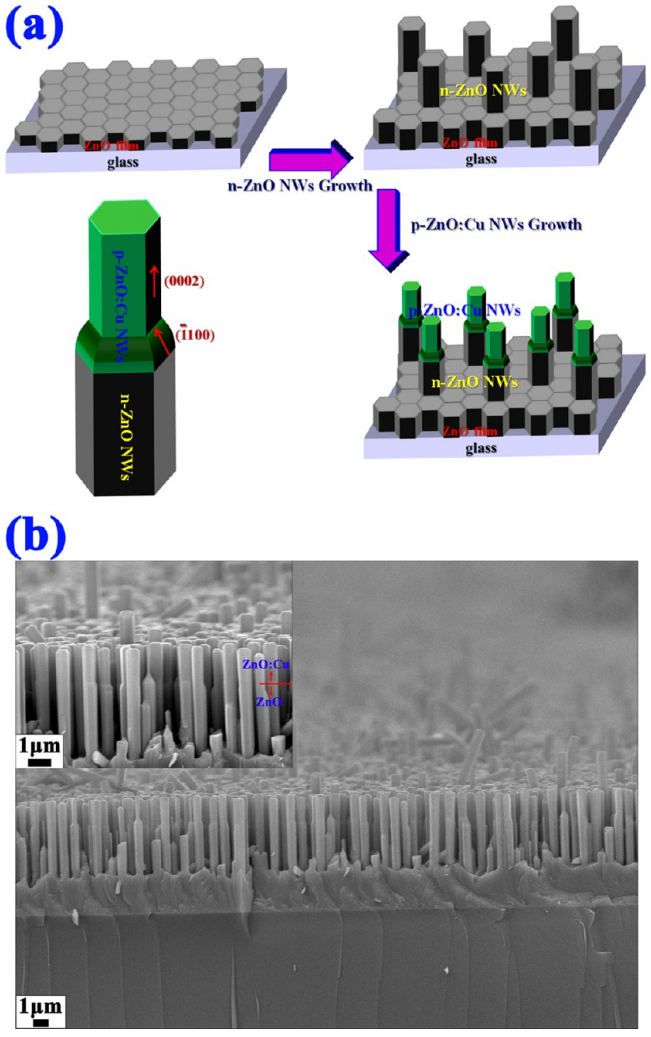

Figure 7. (a) p-ZnO:Cu/n-ZnO homojunction NW growth and processing step. (b) Cross-sectional FESEM images of the p-ZnO:Cu/n-ZnO NWs. The insets in left- and right-hand corners are the magnified image and EDX spectrum, respectively.

homojunction NWs contain approximately 3.68 atomic % Cu by the EDX spectrum measured. However, this image reveals that the majority of Cu elements are distributed in the right side of the NW region. The right side is the top region of the p-ZnO:Cu/n-ZnO NW. Figure 8b offers the HRTEM image of the top-side wall region of the p-ZnO:Cu/n-ZnO NW. The top side of the NW is the p-ZnO:Cu region, which consists of structurally uniform single crystals. The inset in the top-right-hand corner of Figure 8b shows the selected area electron diffraction (SAED) image, which confirmed that the top region of the p-ZnO:Cu region is a single crystal of wurtzite structure. This measured result is consistent with the XRD measured. The HRTEM images demonstrated that the p-ZnO:Cu region is a well-oriented crystal with no obvious defect. The HRTEM image of the p-ZnO:Cu region presents vertical p-ZnO:Cu/n-ZnO homojunction NWs, which are all [0001] growth-oriented, with lateral surfaces enclosed by $(\bar{1}101)$ planes. This is hardly surprising because $(\bar{1}101)$ planes give rise to large facets in ZnO NW growth.

Some papers have suggested that dopant causes the crystallographic defects, such as vacancy defects, interstitial defects, Frenkel defects, dislocations, and stacking faults. These

dx.doi.org/10.1021/am406030d | ACS Appl. Mater. Interfaces 2014, 6, 4277–4285

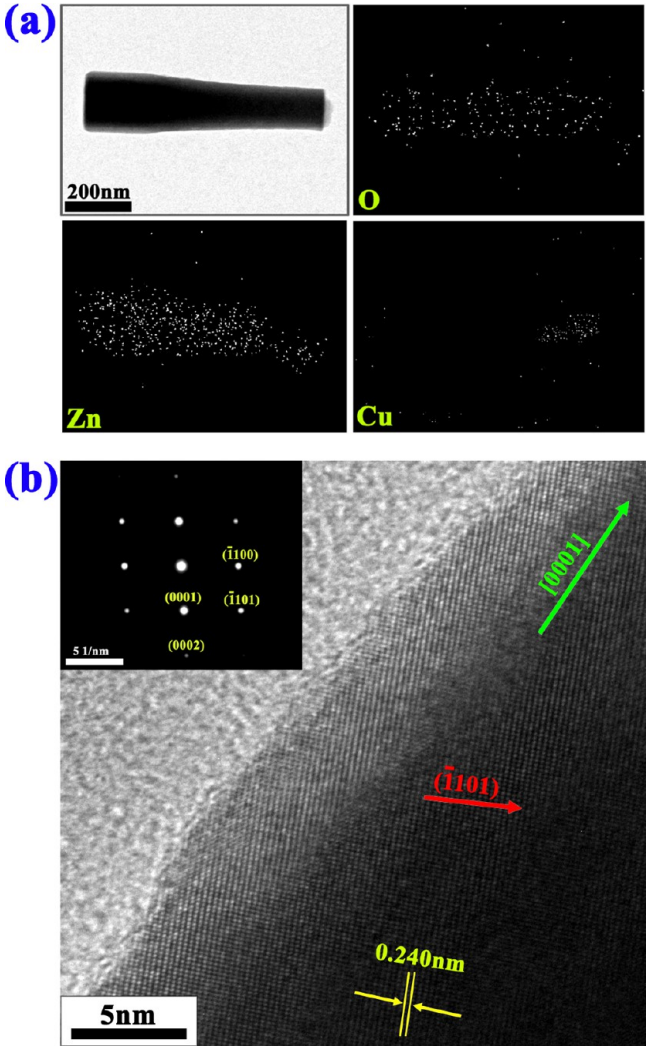

Figure 8. (a) Cross-sectional TEM and EDX mapping images. (b) HRTEM images of the p-ZnO:Cu region. The inset displays SAED images.

crystallographic defects induced ZnO to form other crystal plane growth ratios faster than the (002) plane, thereby affecting the surface of ZnO nanostructure morphology. Because the ZnO:Cu NWs maintained a straight vertical morphology, this provides evidence that the Cu dopant is not the major factor to reduce the diameter of the p-ZnO:Cu region. According to past reports, the furnace heating rate was reported to affect the ZnO nanostructure morphology.[35] In this study, the temperature of the furnace is very important, with an accurate control deviation of 1 °C. By the way, the ZnO/glass substrate was placed on an alumina boat, whose position was kept at the same horizontal level and heated to the same temperature as the Zn vapor source. This was performed to maintain the flow stability, enabling the oxygen and zinc vapors to flow in a horizontal direction as much as possible, thus ensuring that the ZnO NW growth could be maintained in the vertical direction, as displayed in Figure 9a. When the furnace temperature rose to 600 °C after 10 min, the hotwire heater was turned on. The Ta hotwire temperature rose rapidly to 1700 °C, of which the sudden rapid heating caused the entire furnace tube flow to instantly generate a temporary and very unstable condition, as shown in Figure 9b. The unstable flow temporarily increased ($\bar{1}101$) the plane growth ratio and caused

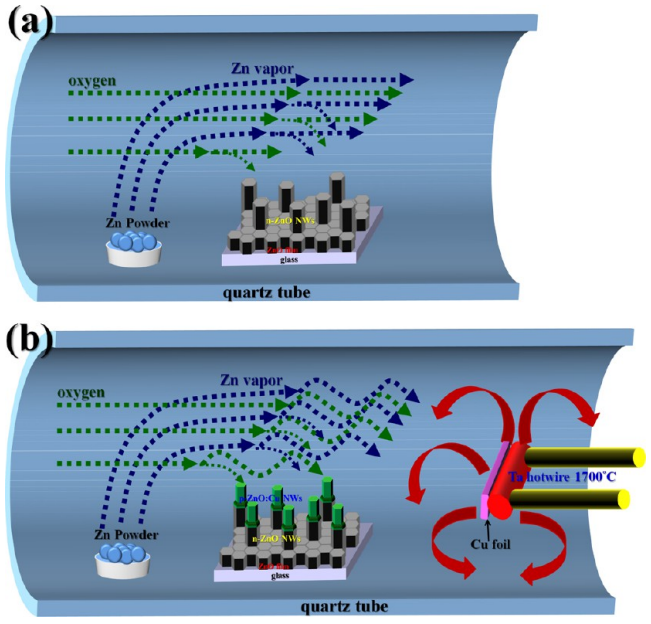

Figure 9. (a) Schematic depiction of the oxygen and zinc vapor flow in the furnace. (b) Rapid rise of hotwires to 1700 °C, causing temporary unstable flow.

the diameter of the p-ZnO:Cu region to narrow. After some time, the hotwire maintained at 1700 °C achieved thermal equilibrium in the furnace tube. The flow then stabilized, and favorable growth in the *c*-axis [0001] lattice-oriented occurred. The p-ZnO:Cu NWs displayed vertical growth along the narrower diameter, which was caused by the temporarily unstable flow.

Figure 10a plots that *I*−*V* curve of the p-ZnO:Cu/n-ZnO homojunction NWs measured under UV exposure and in the dark. The UV light source is a hand-held lamp (λ = 365 nm, ~0.25 mW/cm^2). The *I*−*V* curve displays the characteristics of normal rectifying diodes. The current was measured by scanning voltage bias (from −10 to +10 V) in the dark or under UV exposure. The response increased with both the forward and reverse voltages. In a dark environment, the turn-on voltage, forward current (bias of 10 V), and reverse leakage current (bias −10 V) were 3.63 V, 6.32 × 10^{-6} A, and 4.65 × 10^{-7} A, respectively. The forward and reverse currents under UV illumination clearly exceeded that in the dark. Under UV exposure, the turn-on voltage, forward current (bias of 10 V), and reverse leakage current (bias of −10 V) were 4.68 V, 8.21 × 10^{-6} A, and 2.82 × 10^{-6} A, respectively. The UV illumination forward current (bias of 10 V) and reverse leakage current (bias of −10 V) were almost 1.29 and 6.06 times greater than the measured dark current, respectively. UV exposure was an excitation source to increase the photocurrent. The UV sensing of the reverse bias is more sensitive to the higher ratio than that of the forward bias. Figure 10b presents the measured photoresponse of a homojunction NW photodetector as a function of time when switching the UV lamp on and off in the ambient environment. The I_{dark} and I_{UV} were about 1.12 × 10^{-7} and 6.02 × 10^{-7} A at −5 V reverse bias. Continuous testing established the stability and reproducibility of the homojunction NW photodetector. The I_{UV} was almost 6 times higher than I_{dark} at −5 V. The performance of the photoresponse suffices and applies in a commercial prototype UV photodetector.

dx.doi.org/10.1021/am406030d | ACS Appl. Mater. Interfaces 2014, 6, 4277−4285

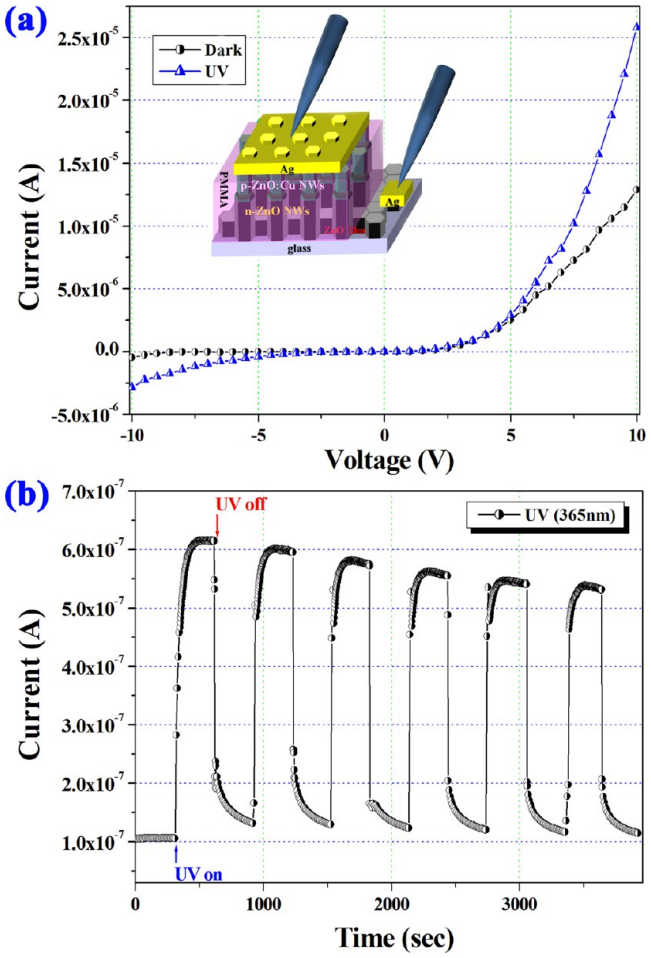

Figure 10. (a) I–V measurements of the p-ZnO:Cu/n-ZnO NWs measured in the dark and under UV exposure. (b) Transient response of the phototransistor with the UV excitation switched on and off.

In this investigation, the photodetector was often operating under reverse bias for the photoconductive mode of the photodiode. The reverse bias increased the depletion width to reduce the response time, homojunction capacitance, and loss of carriers. The equation of the built-in voltage V_{bi} is

$$V_{bi} = \frac{kT}{q} \ln\left(\frac{N_A N_D}{n_i^2}\right)$$

where kT/q is the thermal voltage at 300 K, k is the Boltzmann constant, T is the absolute temperature, N_A and N_D are the number of ionized donors and acceptors, respectively, and n_i is the intrinsic carrier concentration. However, the intrinsic carrier concentration of ZnO is roughly 10^6 cm^{-3} at room temperature. The N_A value was about 10^{16} cm^{-3} by Cu doping, while on the basis of a past report, the N_D value was found to be around 10^{15} cm^{-3}.[9] The turn-on voltage is decided by the built-in voltage V_{bi}, which was calculated to be 1.093 eV. The depletion width W is expressed as

$$W \approx \left[\frac{2\varepsilon_r\varepsilon_0}{q}\left(\frac{1}{N_A} + \frac{1}{N_D}\right)(V_{bi} - V_{applied})\right]^{1/2}$$

where ε_r is the dielectric permittivity of ZnO (~8.86) and $V_{applied}$ is the applied bias. The depletion width W is around 1.086, 2.563, and 3.458 μm with an applied bias of 0, −5, and −10 V, respectively.

Figure 11 presents that energy band diagram of the homojunction NWs with a reverse bias of −5 V. Generally,

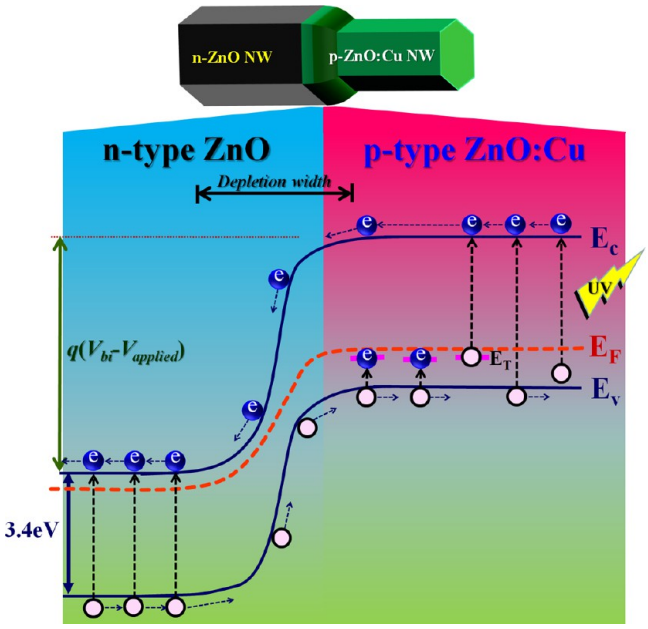

Figure 11. Band diagrams of the p-ZnO:Cu/n-ZnO homojunction NWs.

the Fermi level (E_F) of a n-type ZnO region shifts near the E_C edge. The ZnO:Cu region exhibited p-type characteristics, and its E_F shifted close to the E_V because the O_2^- molecules increased the concentration of holes. Dopant Cu impurities caused a deep level (E_T) in the p-ZnO:Cu region.[5] The energy of a photon (365 nm, 3.397 eV) exceeds the ZnO band gap, ~3.3 eV. These photons have been absorbed in ZnO and then produced electron–hole pairs. Therefore, the O_2^- molecules were removed and become oxygen by absorption holes on the NW surface, while these excited and remaining electrons in the E_C highly improve n-ZnO conductivity and slightly increase p-ZnO:Cu conductivity.

$$O_2^- + h^+ \rightarrow O_{2(gas)}$$

The n-ZnO depletion region disappears nearly clean because the surface O_2^- molecules were remove by UV exposure. Upon such exposure, photons cause many electrons to excite from E_V or E_T and jump to E_C. Generally, the conductivity of a semiconductor can be expressed as

$$\sigma = nq\mu_e + pq\mu_p$$

where n denotes the number density of electrons, q represents the electron charge, μ_e refers to the electron mobility, and μ_p is the hole mobility. It was found that some photoexcited electrons in the p-ZnO:Cu region passed through the p–n homojunction to the n-ZnO region when excited by UV in an electric field.

CONCLUSION

In this study, vertical ZnO:Cu NWs and p-ZnO:Cu/n-ZnO homojunction NWs were grown on a ZnO/glass substrate by a 600 °C furnace with hotwire assistance. In the ZnO:Cu NW

dx.doi.org/10.1021/am406030d | ACS Appl. Mater. Interfaces 2014, 6, 4277–4285

investigation, EDX spectra indicated that the Cu content of hotwires at 1400 and 1700 °C is 1.93 and 3.01 atomic %. The XRD peaks of ZnO shifting to larger angles increase with an increasing amount of doped Cu, which is due to the ionic radius of Cu^{2+} (0.73 Å) being smaller than that of Zn^{2+} (0.74 Å). The Cu dopant enhanced the PL green band peak and increased the ionized oxygen vacancy in ZnO. According to the *I*−*V* measurement, the Cu dopant decreased the conductivity of NWs. The Hall effect and gas sensing measurement verified that all ZnO:Cu NWs were p-type. In this p-ZnO:Cu/n-ZnO homojunction NW study, TEM and EDX mapping images revealed that the majority of Cu elements was distributed at the top of the NWs. The HRTEM image of the p-ZnO:Cu region shows that the NWs are [0001] growth-oriented, with lateral surfaces enclosed by $(\bar{1}101)$ planes. The Ta hotwire temperature rose rapidly to 1700 °C, causing the resultant unstable flow to temporarily increase the $(\bar{1}101)$ plane growth ratio, leading to the diameter of the p-ZnO:Cu region to narrow. The *I*−*V* curve of the p-ZnO:Cu/n-ZnO NWs shows the characteristics of normal rectifying diodes. Lastly, the UV sensing of the reverse bias is more sensitive to the higher ratio than is that of the forward bias. The photocurrent was around 6 times larger than the dark current at −5 V.

AUTHOR INFORMATION

Corresponding Authors

*E-mail: clhsu@mail.nutn.edu.tw.
*E-mail: tingjen1123@yahoo.com.tw.

Notes

The authors declare no competing financial interest.

ACKNOWLEDGMENTS

The authors thank the National Science Council of the Republic of China, Taiwan, for financially supporting this research under Contract NSC 102-2221-E-024-017.

REFERENCES

(1) Hsu, C. L.; Chen, K. C. Improving piezoelectric nanogenerator comprises ZnO nanowires by bending the flexible PET substrate at low vibration frequency. *J. Phys. Chem. C* **2012**, *116*, 9351−9355.
(2) Soci, C.; Zhang, A.; Xiang, B.; Dayeh, S. A.; Aplin, D. P. R.; Park, J.; Bao, X. Y.; Lo, Y. H.; Wang, D. ZnO nanowire UV photodetectors with high internal gain. *Nano Lett.* **2007**, *7*, 1003−1009.
(3) Hsu, C. L.; Tsai, T. Y. Fabrication of fully transparent indium-doped ZnO nanowire field-effect transistors on ITO/glass substrates. *J. Electrochem. Soc.* **2011**, *158*, K20−K23.
(4) Baxter, J. B.; Walker, A. M.; vanOmmering, K.; Aydil, E. S. Synthesis and characterization of ZnO nanowires and their integration into dye-sensitized solar cells. *Nanotechnology* **2006**, *17*, S304−S312.
(5) Hsu, C. L.; Chen, K. C.; Tsai, T. Y.; Hsueh, T. J. Fabrication of gas sensor based on p-type ZnO nanoparticles and n-type ZnO nanowires. *Sens. Actuators, B* **2013**, *182*, 190−196.
(6) Gautam, U. K.; Panchakarla, L. S.; Dierre, B.; Fang, X. S.; Bando, Y.; Sekiguchi, T.; Govindaraj, A.; Golberg, D.; C. Rao, N. R. Solvothermal synthesis, cathodoluminescence, and field-emission properties of pure and n-doped ZnO nanobullets. *Adv. Funct. Mater.* **2009**, *19*, 131−140.
(7) Hsu, C. L.; Chang, S. J.; Lin, Y. R.; Tsai, S. Y.; Chen, I. C. Vertically well aligned p-doped ZnO nanowires synthesized on ZnO−Ga/glass templates. *Chem. Commun.* **2005**, 3571−3573.
(8) Sun, M. H.; Zhang, Q. F.; Wu, J. L. Electrical and electroluminescence properties of As-doped p-type ZnO nanorod arrays. *J. Phys. D: Appl. Phys.* **2007**, *40*, 3798−3802.
(9) Yang, Y.; Qi, J. J.; Liao, Q. L.; Zhang, Y.; Tang, L. D.; Qin, Z. Synthesis and characterization of Sb-doped ZnO nanobelts with single-side zigzag boundaries. *J. Phys. Chem. C* **2008**, *112*, 17916−17919.
(10) Zhu, B. L.; Xie, C. S.; Zeng, D. W.; Song, W. L.; Wang, A. H. Investigation of gas sensitivity of Sb-doped ZnO nanoparticles. *Mater. Chem. Phys.* **2005**, *89*, 148−153.
(11) Baskoutas, S.; Bester, G. Conventional optics from unconventional electronics in ZnO quantum dots. *J. Phys. Chem. C* **2010**, *114*, 9301−9307.
(12) Pan, H. L.; Yao, B.; Yang, T.; Xu, Y.; Zhang, B. Y.; Liu, W. W.; Shen, D. Z. Electrical properties and stability of p-type ZnO film enhanced by alloying with S and heavy doping of Cu. *Appl. Phys. Lett.* **2010**, *97*, 142101.
(13) Kim, J. B.; Byun, D.; Ie, S. Y.; Park, D. H.; Choi, W. K.; Choi, J. W.; Angadi, B. Cu-doped ZnO-based p−n hetero-junction light emitting diode. *Semicond. Sci. Technol.* **2008**, *23*, 095004.
(14) Georgekutty, R.; Seery, M. K.; Pillai, S. C. A highly efficient Ag−ZnO photocatalyst: Synthesis, properties, and mechanism. *J. Phys. Chem. C* **2008**, *112*, 13563−13570.
(15) Hongsith, N.; Viriyaworasakul, C.; Mangkomtong, P.; Mangkorntong, N.; Choopun, S. Ethanol sensor based on ZnO and Au-doped ZnO nanowires. *Ceram. Interfaces* **2008**, *34*, 823−826.
(16) Xing, G. Z.; Yi, J. B.; Tao, J. G.; Liu, T.; Wong, L. M.; Zhang, Z.; Li, G. P.; Wang, S. J.; Ding, J.; Sum, T. C.; Huan, C. H. A.; Wu, T. Comparative study of room-temperature ferromagnetism in Cu-doped ZnO nanowires enhanced by structural inhomogeneity. *Adv. Mater.* **2008**, *20*, 3521−3527.
(17) Buchholz1, D. B.; Chang, R. P. H.; Song, J. Y; Ketterson, J. B. Room-temperature ferromagnetism in Cu-doped ZnO thin films. *Appl. Phys. Lett.* **2005**, *87*, 082504.
(18) Gong, H.; Hu, J. Q.; Wang, J. H.; Ong, C. H.; Zhu, F.R. Nanocrystalline Cu-doped ZnO thin film gas sensor for CO. *Sens. Actuators, B* **2006**, *115*, 247−251.
(19) Lupan, O.; Pauporte, T.; Le Bahers, T.; Viana, B.; Ciofini, I. Wavelength-emission tuning of ZnO nanowire-based light-emitting diodes by Cu doping: Experimental and computational insights. *Adv. Funct. Mater.* **2011**, *21*, 3564−3572.
(20) Kanai, Y. Admittance spectroscopy of Cu-doped ZnO crystals. *J. Appl. Phys.* **1991**, *30*, 703−707.
(21) Xu, C. X.; Sun, X. W.; Zhang, X. H.; Ke, L.; Chua, S. J. Photoluminescent properties of copper-doped zinc oxide nanowires. *Nanotechnology* **2004**, *15*, 856−861.
(22) Sun, H.; Zhang, Q. F.; Wu, J. L. Electroluminescence from ZnO nanorods with an n-ZnO/p-Si heterojunction structure. *Nanotechnology* **2006**, *17*, 2271−2274.
(23) Chen, C. H.; Chang, S. J.; Chang, S. P.; Li, M. J.; Chen, I C.; Hsueh, T. J.; Hsu, A. D.; Hsu, C. L. Fabrication of a white-light-emitting diode by doping gallium into ZnO nanowire on a p-GaN substrate. *J. Phys. Chem. C* **2010**, *114*, 12422−12426.
(24) Luo, L.; Sosnowchik, S. D.; Lin, L. W. Room temperature fast synthesis of zinc oxide nanowires by inductive heating. *Appl. Phys. Lett.* **2007**, *90*, 093101.
(25) Chrissanthopoulos, A.; Baskoutas, S.; Bouropoulos, N.; Dracopoulos, V.; Poulopoulos, P.; Yannopoulos, S.N. Synthesis and characterization of ZnO/NiO p−n heterojunctions: ZnO nanorods grown on NiO thin film by thermal evaporation. *Photonics Nanostruct. Fundam. Appl.* **2011**, *9*, 132−139.
(26) Look, D. C.; Claflin, B. p-Type doping and devices based on ZnO. *Phys. Status Solidi B* **2004**, *241*, 624−630.
(27) Chen, M. T.; Lu, M. P.; Wu, Y. J.; Song, J. H.; Lee, C. Y.; Lu, M. Y.; Chang, Y. C.; Chou, L. J.; Wang, Z. L.; Chen, L. J. Near UV LEDs made with in situ doped p−n homojunction ZnO nanowire arrays. *Nano Lett.* **2010**, *10*, 4387−4393.
(28) Leung, Y. H.; He, Z. B.; Luo, L. B.; Tsang, C. H. A.; Wong, N. B.; Zhang, W. J.; Lee, S. T. ZnO nanowires array p−n homojunction and its application as a visible-blind ultraviolet photodetector. *Appl. Phys. Lett.* **2010**, *96*, 053102.
(29) Fang, X.; Li, J. H.; Zhao, D. X.; Shen, D. Z.; Li, B. H.; Wang, X. H. Phosphorus-doped p-type ZnO nanorods and ZnO nanorod p−n

homojunction LED fabricated by hydrothermal method. *J. Phys. Chem. C* **2010**, *113*, 21208−21212.
(30) Lyu, S. C.; Zhang, Y.; Ruh, H.; Lee, H. J.; Shim, H. W.; Suh, E. K.; Lee, C. J. Low temperature growth and photoluminescence of well-aligned zinc oxide nanowires. *Chem. Phys. Lett.* **2002**, *363*, 134−138.
(31) Jin, B. J.; Bae, S. H.; Lee, S. Y.; Im, S. Effects of native defects on optical and electrical properties of ZnO prepared by pulsed laser deposition. *Mater. Sci. Eng., B* **2000**, *71*, 301−305.
(32) Barsan, N.; Schweizer-Berberich, M.; Gopel, W. Fundamental and practical aspects in the design of nanoscaled SnO_2 gas sensors: A status report. *Fresenius' J. Anal. Chem.* **1999**, *365*, 287−304.
(33) Park, M. S.; Min, B. I. Ferromagnetism in ZnO codoped with transition metals: $Zn_{1-x}(FeCo)_xO$ and $Zn_{1-x}(FeCu)_xO$. *Phys. Rev. B: Condens. Matter Mater. Phys.* **2003**, *68*, 224436.
(34) Spaldin, N. A. Search for ferromagnetism in transition-metal-doped piezoelectric ZnO. *Phys. Rev. B: Condens. Matter Mater. Phys.* **2004**, *69*, 125201.
(35) Hsu, C. L.; Yang, S. S.; Tseng, Y. K.; Chen, I. C.; Lin, Y. R.; Chang, S. J.; Wu, S. T. A new and simple means for self-assembled nanostructure: Facilitated by buffer layer. *J. Phys. Chem. B* **2004**, *108*, 18799−18803.